CrossMark

ORIGINAL ARTICLE

Behavior of concrete columns reinforced with high-strength steel rebars under eccentric loading

Sayedmahdi Alavi-Dehkordi [iD] · **Davood Mostofinejad**

Abstract In this study, high-strength steel (HSS) reinforcement with a yield stress of about 600 MPa was used in reinforced concrete columns to reduce both the reinforcing bar congestion and the construction costs. For this purpose, 16 square concrete columns reinforced with either the conventional normal-strength steel (NSS) or HSS rebars were subjected to axial and eccentric compression loads. The primary test variables included longitudinal reinforcement with two strength grades, axial load eccentricities, two different concrete compressive strengths, and different longitudinal reinforcement ratios. The structural response of the columns reinforced with reduced HSS rebars (Grade 600) was compared with that of the columns reinforced with grade 420 MPa rebars in terms of their load-carrying capacity, failure mechanism, axial force-bending moment (P-M) interaction, and ductility. Experimental results showed that although the amount of longitudinal steel reinforcement was reduced by about 34% in columns containing grade 600 MPa rebars, their load-carrying capacity and P–M interaction diagrams were comparable to those of the reference

columns containing conventional NSS rebars. It was also concluded that simultaneous use of high-strength rebars and high-strength concrete below a balanced point would lead to slightly higher values of ductility index (by up to 4%) than when normal concrete strength and conventional reinforcement steel rebars of Grade 420 MPa are used.

Keywords High-strength steel (HSS) · Eccentric loading · Reinforced concrete column · High-strength concrete · Ductility · P–M interaction diagram

1 Introduction

Recently, the use of high strength steel reinforcement in reinforced concrete (RC) structures, especially in high-rise buildings, has attracted a great attention due to the role it plays in alleviating the reinforcement congestion problem that is the principal cause of such difficulties as formidable concrete casting, honeycombed concrete surface, and difficult concrete consolidation during the construction. Although the use of high-strength steel (HSS) bars to decrease reinforcement volume has been mainly practiced as a remedy to the bar congestion problem in the seismic design of RC elements, their use in ordinary RC structures also offers the potential to reduce construction costs, steel manufacturing energy consumption, and the adverse

S. Alavi-Dehkordi (✉) · D. Mostofinejad
Department of Civil Engineering, Isfahan University of Technology (IUT), Isfahan 84156-83111, Iran
e-mail: alavi.sayedmahdi@gmail.com;
m.alavi@alumni.iut.ac.ir

D. Mostofinejad
e-mail: dmostofi@cc.iut.ac.ir

environmental impacts of the construction industry. Moreover, their high yield strength, good weldability, good bendability, and reasonable elongation properties make HSS rebars a highly desirable replacement for conventional steel rebars to achieve a more economical structural system.

On the other hand, the higher strain of high-strength steel may cause early concrete crushing in the compression zone of RC columns prior to the yield strain of HSS bars [1]. In this case, full column strength cannot be exploited. To this may be added the disadvantage of reduced member ductility since, for a given rebar size, a larger compressive force developed in HSS bars may increase the likelihood of rebar buckling in RC columns. Finally, it is known that the performance of a member governed by flexure depends to a great extent on the longitudinal reinforcement index defined as $\rho_s \cdot f_y/f'_c$, where ρ_s is the steel reinforcement ratio, and f_y and f'_c are the yield strength of steel bars and the compressive strength of concrete, respectively. Hence, the lower longitudinal reinforcement ratio in concrete columns reinforced with HSS bars potentially affects the load-carrying capacity, flexural performance, and post-peak behavior of eccentrically loaded columns.

High strength steel bars were first used in RC columns by Richart and Brown [2]. These authors used longitudinal rebars with a steel yield strength of 660 MPa and a well-defined yield plateau in eight spirally reinforced columns to show that even such rebars used in RC columns with a circular cross-section would be fully effective in resisting concentric axial compression. Later, Pfister et al. [3] conducted a test program on concentrically loaded columns reinforced with bars of yield strengths in the range of 628 to 642 MPa. The results showed that the yield point of longitudinal bars could only be extended to the ultimate strength of the tied column at a strain equal to 0.003 mm/mm or less. This can be more readily achieved by well-defined yield plateau bars having a nearly linear stress–strain curve up to the yield point rather than by bars lacking a definitive yield point [3].

Todeschini et al. [4] extended Richart and Brown's research and their findings indicated that a stress range of 480 to 550 MPa could be developed in reinforcement bars lacking a well-defined yield plateau while stresses up to 620 MPa could be developed in those having a relatively flat yield plateau. Nagashima et al.

[5] examined squared RC columns which were reinforced with 400–800 MPa longitudinal bars and 800–1400 MPa transverse reinforcements. They reported that the higher yield strength of longitudinal bars had an insignificant effect on stress–strain relationship of columns.

For years, structural concrete designs were restricted to reinforcing rebars with the given yield strength, f_y, of 420 MPa or less. This limit was later raised to 550 MPa for all reinforcement steel rebars in ACI 318-71 [6]. The current US design codes still limit maximum allowable yield stress to 550 MPa for all steel reinforcements, except for those used as confinement rebars with a maximum of 690 MPa and those used to resist earthquake-induced forces with a maximum limited to 420 MPa [7].

In 2010, the ACI Innovation Task Group (ITG-6R-10) [8] published the report titled "Design guide for the use of grade 690 MPa steel bars for structural concrete", in which the maximum compressive stress of longitudinal reinforcement used in members subjected to axial loading is limited to 550 MPa. The steel strain, ε_s, corresponding to this stress is approximately 0.0028, which is nearly equal to the maximum strain (0.003) for concrete in compression allowed by ACI 318-08 [9]. According to this guideline, the maximum value of f_y in members subjected to axial load combined with a moment should be restricted to 550 MPa for the longitudinal reinforcement subjected to compression, and to 690 MPa for the longitudinal reinforcement subjected to tension.

Based on stress–strain relations for normal-weight concrete, both strain at peak compressive stress (ε_{co}) and ultimate compressive strain (ε_{cu}) increase slightly with increasing concrete compressive strength (f'_c) [10]. This shows the higher potential of high strength concrete to be reinforced with HSS bars due to their better strain compatibility. In addition to the excellent mechanical performance and durability of HSC, Shin et al. [10] have demonstrated the positive effects of the combination use of high-strength longitudinal reinforcement and high strength concrete in RC column on improving the strength of composite columns and the resulting yielding point of HSS longitudinal bars. However, the beneficial effect of HSS longitudinal bar on axial load capacity of columns with ultra-high strength concrete could decrease significantly due to

the sudden spalling of the concrete cover and the low contribution of HSS bars to column load capacity [10].

Our literature review indicates that most experimental studies were focused on the use of HSS bars in concentrically loaded RC columns with high yield strength transverse reinforcement [11–14], ignoring those reinforced with high strength longitudinal reinforcement subjected to eccentric loading. The present study, therefore, aims to explore the effects of reduced amounts of high strength longitudinal bars (600 MPa) on the axial load-carrying capacity, flexural strength, load–displacement behavior, and ductility of columns. The results will then be compared with obtained from counterpart columns reinforced with grade 420 MPa - bars. More specifically, well-confined RC columns will be tested under increasing monotonic concentric and eccentric compression loading applied at different load eccentricities in order to determine the failure mechanisms as well as the axial load–bending moment (P–M) interaction diagrams for columns containing different concrete and reinforcement grades. The results of this study may facilitate the use of HSS in reinforced concrete members for practical engineers in order to both reduce the congestion of the reinforcing bars and decrease the total expenses.

2 Experimental program

For the purposes of this study, sixteen RC columns with cross sections of 133×133 mm and overall heights of 500 mm were prepared and tested to gain insight into the behavior of practical-sized columns reinforced with HSS (Grade 600) bar. The relatively small height and cross-section of the RC columns were selected due to restrictions in the test equipment and instruments available in the laboratory. Half the experimental specimens were reinforced with four 10-mm conventional normal-strength steel (NSS) longitudinal rebars (420 MPa) to give a longitudinal reinforcement ratio of 1.78%, while the remaining eight were reinforced with four 8-mm longitudinal HSS deformed bars (600 MPa) with a longitudinal reinforcement ratio of 1.13%. The ratios met the minimum longitudinal reinforcement ratios required by the latest ACI 318 [7].

As shown in Fig. 1, all the experimental specimens were also laterally reinforced with normal strength deformed 8-mm bars with a yield strength of 425 MPa. Moreover, all the specimens were laterally confined uniformly as per ACI 318-14 code [7], and transverse bars in all were spaced at distances of 53.8 mm from the center. Thus, the volumetric ratio of lateral ties was kept constant at 4% in all the sixteen RC columns.

The clear concrete cover in all the specimens measured 20 mm from the outside of the perimeter tie. In order to provide an adequate anchorage length, each end of the longitudinal bar was connected to a square steel plate 15 mm thick. Both plates had square holes 47.4 mm wide in the center to allow for easier concrete pouring. Figure 1 presents the details of the specimens and the plates used.

2.1 Material properties

The yield and ultimate strengths of the longitudinal HSS bars were measured to be 600 MPa and 731 MPa, respectively. The same parameters for the 10-mm NSS bars were 417 MPa and 601 MPa, respectively. All the HSS bars used had been manufactured using the "thermex technology" originally developed by Hennigsdorfer Stahl Engg. (HSE) Gmbh, Germany [15]. Table 1 reports the mechanical specifications and tensile test results of the reinforcing bars employed.

In this study, two different levels of concrete strength were used. The normal strength concrete (NSC) mixture was designed according to ACI-211.1 [16] to provide a 28-day compressive strength of 35 MPa. The trial batch method was used to design high strength concrete (HSC) mixture with a compressive strength of 60 MPa. The material used in the concrete mixtures included ordinary Portland cement (Type 1), 0 to 5 mm sand, and 5 to 10 mm crushed gravel as aggregate. Additionally, polycarboxylate superplasticizer was added to the mixture to enhance concrete workability and consolidation. The mix design proportions of both concrete strengths are reported in Table 2. All the column specimens and the cylinders were cast in vertical position on the ground and removed from the mold after 24 h before being cured in the water bath for up to 28 days. Three identical cylindrical concrete specimens 150 mm in diameter and 300 mm in height were also tested according to ASTM C39 [17] to obtain the average concrete compressive strength of each column on the test day.
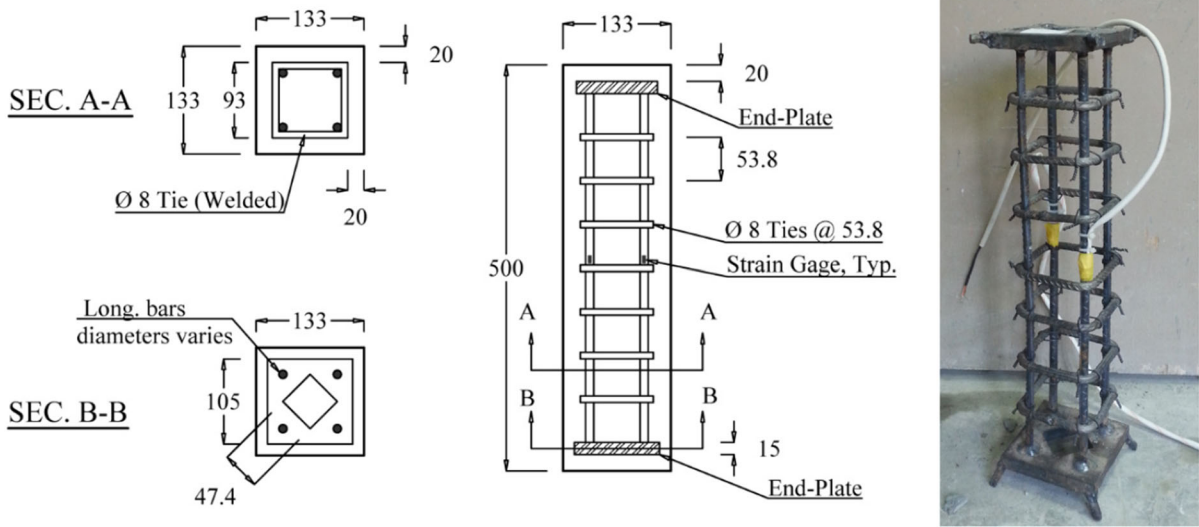
Fig. 1 Reinforcement details (dimensions are in mm)

Table 1 Mechanical properties of steel reinforcements

Bar size (mm)	Diameter (mm)	Bar type	f_y[a] (MPa)	f_u (MPa)	Elastic modulus (MPa)	Total elongation (%)
8	8.1	N[b]	425	633	205,800	28
8	8.1	H[c]	600	731	204,600	18
10	10	N	417	601	201,728	27

[a]All steel bars have well-defined yield plateaus

[b]N refers to normal steel rebars

[c]H refers to high-strength steel rebars

Table 2 Concrete mix proportions (kg/m³)

Concrete type	Normal-strength concrete	High-strength concrete
Fine aggregate	855	635
Coarse aggregate	778	1096
Water	221	168
Cement	422	500
Super-plasticizer	–	4.5
w/c ratio	0.54	0.35
Compressive strength at test day (MPa)	36	62

2.2 Test layout

The 16 RC columns constructed for this experimental program were categorized into two groups. The specimens in the first group were classified into the four categories of C36.N, C36.H, C62.N, and C62.H based on their concrete and rebar grades (Table 3). For instance, The category C36.N includes specimens (C36.N.E0, C36.N.E60, C36.N.E90, C36.N.Ei) made with 36 MPa concrete strength and normal longitudinal steel rebar (Grade 420 MPa). Each category consisted of four specimens meant to be subjected to axial compressive loading with eccentricities of 0, 60 mm, 90 mm, and infinity. The symbols used in

Table 3 Test layout

Category	Specimen code	Longitudinal rebar			Transverse rebar			f_c' (MPa)	Type of loading
		Number-size (mm)	f_{yl} (MPa)	ρ_l (%)	Size (mm)	Space (mm)	f_{yh} (MPa)		
C36.N	C36.N.E0	4–Φ10	420	1.78	Φ8	53.8	420	36	Axial, concentric
	C36.N.E60	4–Φ10	420	1.78	Φ8	53.8	420	36	Axial, e^a = 60 mm
	C36.N.E90	4–Φ10	420	1.78	Φ8	53.8	420	36	Axial, e = 90 mm
	C36.N.Ei	4–Φ10	420	1.78	Φ8	53.8	420	36	Four-point flexural
C36.H	C36.H.E0	4–Φ8	600	1.13	Φ8	53.8	420	36	Axial, concentric
	C36.H.E60	4–Φ8	600	1.13	Φ8	53.8	420	36	Axial, e = 60 mm
	C36.H.E90	4–Φ8	600	1.13	Φ8	53.8	420	36	Axial, e = 90 mm
	C36.H.Ei	4–Φ8	600	1.13	Φ8	53.8	420	36	Four-point flexural
C62.N	C62.N.E0	4–Φ10	420	1.78	Φ8	53.8	420	62	Axial, concentric
	C62.N.E60	4–Φ10	420	1.78	Φ8	53.8	420	62	Axial, e = 60 mm
	C62.N.E90	4–Φ10	420	1.78	Φ8	53.8	420	62	Axial, e = 90 mm
	C62.N.Ei	4–Φ10	420	1.78	Φ8	53.8	420	62	Four-point flexural
C62.H	C62.H.E0	4–Φ8	600	1.13	Φ8	53.8	420	62	Axial, concentric
	C62.H.E60	4–Φ8	600	1.13	Φ8	53.8	420	62	Axial, e = 60 mm
	C62.H.E90	4–Φ8	600	1.13	Φ8	53.8	420	62	Axial, e = 90 mm
	C62.H.Ei	4–Φ8	600	1.13	Φ8	53.8	420	62	Four-point flexural

[a] Applied eccentricity level of loading

designating the specimens are: (1) *E*, representing loading eccentricity; (2) *C*, representing concrete compression strength; (3) *N*, standing for normal-strength steel bar, Grade 420, representing the control specimens; (4) *H*, standing for high-strength steel bar, Grade 600; (5) *i*, standing for infinite eccentricity in specimens subjected to the four-point flexural bending test; (6) the values 0, 60, and 90 denotes the loading eccentricity levels in mm; and (7) the figures 36 and 62 following the letter *C* to indicating the concrete compression strength (in MPa) for normal and high strength concretes, respectively. For example, the specimen C36.H.E60 denotes a column with a concrete strength of 36 MPa reinforced with HSS rebars (Grade 600) and subjected to a loading eccentricity of 60 mm.

The specimens in second group are classified in the four categories of E0, E60, E90, and Ei based on loading eccentricity (in mm) (Table 4). For example, the category E90 includes the columns C36.N.E90, C36.H.E90, C62.N.E90, and C62.H.E90.

2.3 Test setup and instrumentation

The columns subjected to eccentric compression loading were tested using a machine equipped with a 2000-kN hydraulic jack. An especially designed eccentric loading setup was used to transfer the force generated by the hydraulic jack. Initially, an eccentric loading plate, composed of a thick square steel plate and a hump (half cylinder rebar), was welded at the middle of the plate to convert the load applied into a uniform strip load for both the upper and lower ends of the compression jack. The eccentric loading setup consisted of two end caps that were to receive the load from the humps and transfer it to the specimen at the desired eccentricity. The end cap had five grooves on it for eccentricities of zero, 30 mm, 60 mm, 90 mm, and 120 mm (Fig. 2). The eccentric loading test was accomplished by positioning the hump of the loading plate on one of the five grooves corresponding top desired eccentricity. Axial displacements on the tension and compression sides of the column were measured using two linear variable differential transducers (LVDTs) with a gauge length of 20 mm and an accuracy of 0.005 mm on both the tension and

Table 4 Summary of test results

Specimen code	Peak load (kN)	Experimental/ theoretical load capacity	Maximum moment (kN.m)	Compression (tension) strain at peak (%)	Midspan disp. at peak (mm)	Disp. at first yield [a] (mm)	Load at first yield[a] (mm)	Ductility index (I_{10})
Category E0								
C36.N.E0	691.4	1.04	0	0.47	–	0.62	587.3	9.08
C36.H.E0	671.1	1.05	0	0.52	–	0.49	598.6	8.50
C62.N.E0	1178.9	1.13	0	0.32	–	0.68	1145.2	9.11
C62.H.E0	1164.5	1.12	0	0.30	–	0.63	1069.9	8.41
Category E60								
C36.N.E60	188.3	0.96	11.3	0.63 (0.40)	–	0.95	184.0	8.35
C36.H.E60	197.0	1.11	11.8	0.67 (0.48)	–	0.96	195.0	8.58
C62.N.E60	288.7	1.04	17.3	0.71 (0.64)	–	1.20	251.0	8.29
C62.H.E60	284.5	1.07	17.1	0.67 (0.62)	–	1.15	249.0	7.24
Category E90								
C36.N.E90	111.7	0.96	10.1	0.59 (0.68)	–	0.96	96.6	8.19
C36.H.E90	119.9	1.08	10.8	0.66 (0.70)	–	1.06	107.4	7.56
C62.N.E90	151.6	1.06	13.6	0.65 (0.83)	–	0.93	127.6	8.77
C62.H.E90	148.5	1.09	13.4	0.67 (0.78)	–	0.9	117.1	7.88
Category Ei								
C36.N.Ei	94.2	1.01	6.12	–	3.35	1.20	70.1	8.68
C36.H.Ei	105.8	1.23	6.88	–	3.85	1.19	66.8	8.14
C62.N.Ei	113.1	1.04	7.35	–	4.07	1.20	79.4	8.17
C62.H.Ei	111.8	1.10	7.26	–	4.12	1.01	67.1	8.46

[a]Recorded by the strain gauges installed at mid-length of longitudinal rebars

compression sides. These vertical LVDTs had been mounted on a particular frame close to the column surface at column mid-height.

The yield points of the longitudinal reinforcements were determined using two electrical strain gauges installed on two opposing points at the mid-height of the tension and compression longitudinal rebars (Fig. 1). As seen in the instrumentation setup in Fig. 2, a gap was inevitably made between the column surface and the LVDTs. The readings were, therefore, corrected using the linear interpolation method.

Pure bending strength was obtained for each experimental RC column by applying a four-point flexural loading using a hydraulic test machine with a capacity of 600 kN. One load cell with a capacity of 300 kN was also installed to measure the load transferred to the specimen, and one LVDT with an accuracy of 0.01 mm was placed under the specimen

to measure midspan displacement. Displacement control was practiced at a rate of 1.0 mm per minute for all the 16 experimental specimens. The test setup and instrumentation used for the four-point flexural loading are shown in Fig. 3.

3 Experimental results

3.1 General column behavior

Figure 4 shows the applied load versus axial displacement curves of both concentrically and eccentrically loaded columns. In addition, the load versus mid-span deflection curves for the columns subjected to the four-point flexural bending test are presented in the same figure. The load–displacement curves for the concentrically loaded columns were derived using the
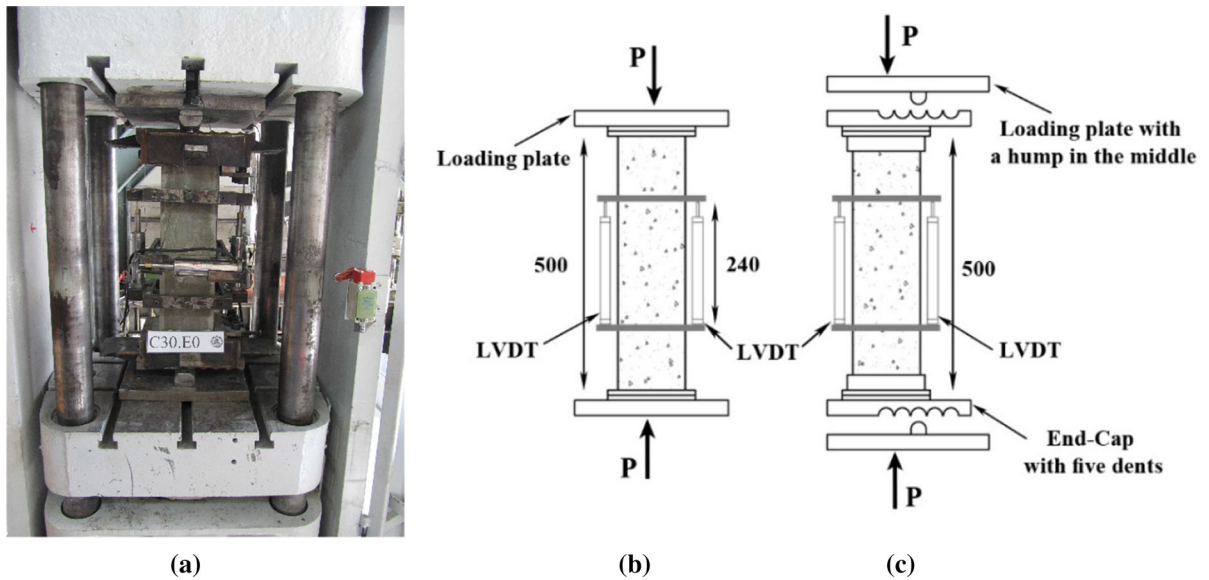
Fig. 2 **a** Column testing machine and instrumentation; **b** setup for concentrically-loaded columns; **c** setup for eccentrically-loaded columns (dimensions are in mm)

average values of axial displacement measured by the two LVDTs installed on both sides of the column (Fig. 2). Figure 4 presents the positive and negative values of axial displacement on the compression and tension sides for the eccentric columns, respectively.

Load–displacement curves consisted of two main branches: an ascending and a descending one. Clearly,
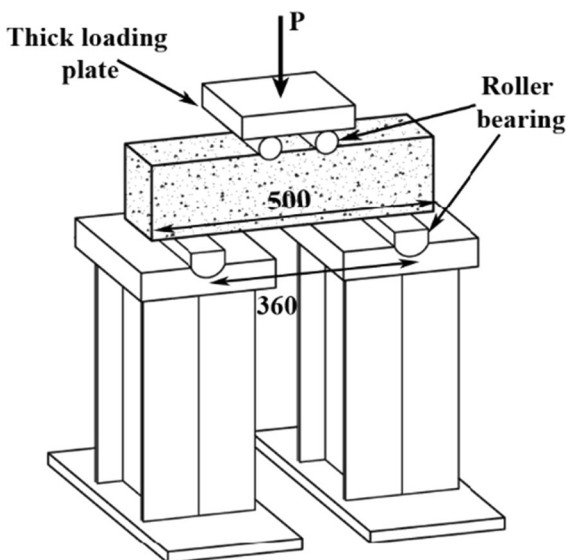
Fig. 3 Test setup and instrumentation used for four-point flexural loading (dimensions are in mm)

the main initial component of the ascending branch initiated at the origin and grew in a linear manner up to loadings of approximately 50% to 90%. The initial axial stiffness decreased with increasing load eccentricity followed by a semi-linear ascending phase that developed at a lower rate up to the peak load. As a result of crack propagation on the compression and flexural-tension sides (depending on the eccentricity level applied) and the consequent concrete cover spalling, initial stiffness in the specimens decreased gradually. Specimens with higher concrete compressive strengths exhibited moderately higher values of initial stiffness and steeper ascending parts in their load–displacement curves. When the peak load was reached, higher stresses developed in the concrete core due to crack propagation and concrete cover spalling.

The descending branch initiated after the peak point and was followed by a considerable decrease in load carrying capacity before the concrete gradually deteriorated up to the ultimate failure point. In contrast, the descending branch for the compression-controlled columns (especially for those in the category E0) declined in an abrupt and brittle manner but at varying rates (depending on load eccentricity and concrete compression strength) while the descending branch in for the high eccentrically loaded columns (especially those in the category Ei) declined in a more ductile manner and at a lower rate.
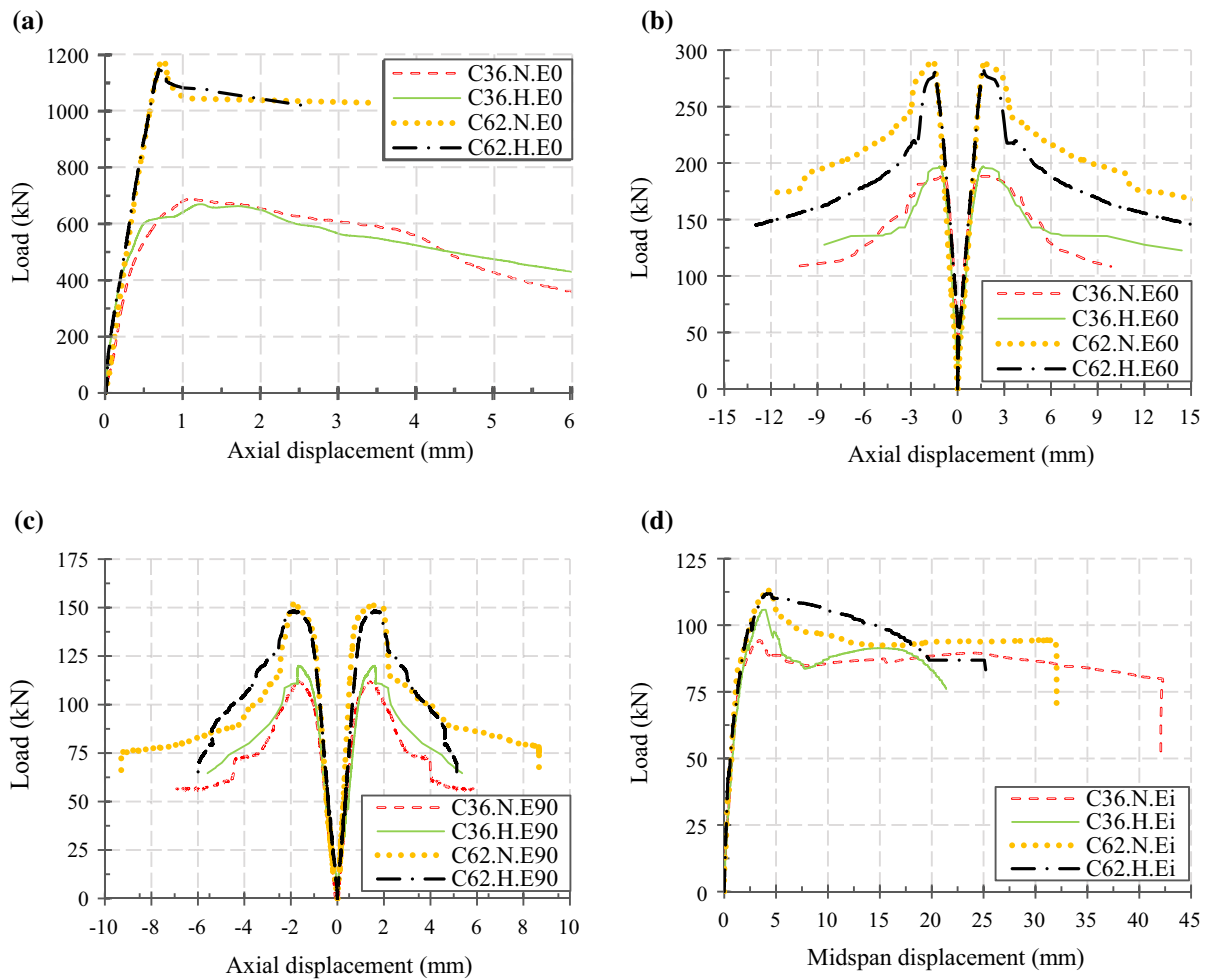
(a)

(b)

(c)

(d)

Fig. 4 Load–displacement curves: **a** category E0; **b** category E60; **c** category E90; and **d** category Ei

The longitudinal reinforcing bars in all the compression controlled columns yielded approximately at 80–95% of the peak load before concrete cover spalling occurred, while the longitudinal tension bars in the tension-controlled specimens yielded at 60–90% of the maximum load before the peak point was reached. Table 4 reports column yield points measured using the strain-gauges installed on opposite positions on the longitudinal bars (Fig. 1).

3.2 Failure mode and load carrying capacity

The mechanical failure mechanism, strain and displacement at peak load, yield point of longitudinal bars, crack pattern, and other load–displacement results obtained for all the tested specimens are

categorized based on the load eccentricity applied and presented in the following four categories:

3.2.1 Category E0

The applied load increased steadily in C36.N.E0 and C36.H.E0 up to load levels of 390 kN (equal to 56% P_{max}) and 340 kN (equal to 51% P_{max}), respectively. At this stage, both specimens exhibited almost equal levels of initial stiffness defined as the angle between the load–displacement curve and the horizontal axis. Beyond this point, hairline cracks initiated at column mid-height and the stress gradually increased to the peak point at a slower rate. In the course of the test, the cracks propagated along the columns and grew longer and wider. As loading progressed, shortly after the

peak point was reached, concrete cover spalling and crushing occurred at column mid-height that caused the specimens to fail.

The loads in the specimens C62.N.E0 and C62.H.E0 were observed to increase linearly following almost identical slopes up to load levels of 860 kN (equal to 73% P_{max}) and 900 kN (equal to 77% P_{max}), respectively. It is worth noting that the increase in concrete compression strength led to a slight increase in the initial stiffness of C62.N.E0 and C62.H.E0 compared to that observed for columns with a concrete strength of 36 MPa.

As the test proceeded, micro-cracks propagated along the columns; indeed, the first major vertical crack appeared at one-third column depth in C62.N.E0 and C62.H.E0 at loads of 924 and 1032 kN, whereas the longitudinal rebars yielded at 0.68 and 0.63 mm, respectively. The onset of cover spalling occurred at the peak point and the existing cracks extended vertically followed by concrete cover splitting. As shown in Fig. 4, the axial strengths of C62.N.E0 and C62.H.E0 dropped significantly at load levels of 1009 and 1017 kN, respectively. The post-peak behavior of these two specimens exhibited slightly brittle failure modes due to the high axial load developed in the columns as a result of the high strength concrete used.

3.2.2 Category E60

Upon loading, horizontal tensile cracks appeared at 144 kN and 157 kN at mid-height of the tension sides in the specimens C36.N.E60 and C36.H.E60, respectively. Initial yielding of tensile rebars in C36.N.E60 and C36.H.E60 were observed at slightly before the peak point at 184 kN and 195 kN, respectively. With increasing eccentric loading, not only did the existing cracks propagate and widen but new cracks also appeared parallel to the axial load applied on the compression side.

Horizontal micro-cracks initiated at 115 kN and 108 kN on the tension side of the specimens C62.H.E60 and C62.H.E60, respectively, followed by the initial yielding of the tensile rebars in these specimens at 251 kN and 249 KN. In all the four specimens in this category, compressive rebars yielded slightly after the peak point had been reached; this was accompanied by concrete cover crushing and splitting, leading finally to concrete cover spalling at column mid-height.

3.2.3 Category E90

Since increased load eccentricity causes the natural axis depth to reduce, horizontal cracks on the tension side of the column appeared and propagated at the lower load level. Horizontal flexural-tension cracks in the specimens subjected to an eccentric loading of 90 mm initiated at column mid-height at 0.1 P_{max} to 0.2 P_{max}, which later grew longer and wider as the applied load gradually increased. As with the specimens in the category E60, the compressive rebars in these specimens yielded at the post-peak point, which was accompanied by a considerable decline in load capacity and concrete crushing.

The failure mechanism in the specimens subjected to eccentric loadings of 60 mm and 90 mm was in the transition mode between compression-controlled and tension-controlled based on ACI 318-14 [7]. This was confirmed by strain gauge records, theoretical calculations, and test-day observations.

3.2.4 Category Ei

Four of the experimental specimens were subjected to the four-point flexural test to investigate the behavior of columns under infinite eccentricity. As shown in Fig. (4), the curves exhibited a rising trend at a monotonous rate up to the yield of the tensile rebars. At the point of maximum load, the concrete crushed at extreme compressive fiber in all the four specimens. As the test proceeded, the load–displacement curves nearly reached their steady state after the load had declined by 6 to 24%, so that strain hardening could be clearly seen in Fig. 4d.

At later stages of the test, the cracks formed in the previous stages increased until the column failed and concrete crushing and failure in all the specimens occurred in a completely mild manner at the middle one-third (i.e., in the zone with constant flexure) of the column height. Examination of the effects of concrete compressive strength on the flexural behavior of C62.H.Ei and C36.H.Ei reveals that the 62 MPa concrete type led to slightly increased initial stiffness and initial slope in the specimen C62.H.Ei. Comparison of the two specimens C62.N.Ei and C36.N.Ei also indicates a slight increase in the initial stiffness and the initial slope of C62.N.Ei.

Test results revealed that the columns C36.H.E0 and C62.H.E0 reinforced with grade 600 MPa rebars were

not significantly different in terms of their maximum loads (only by 2.9% and 1.2%, respectively) from the reference specimens C36.N.E0 and C62.N.E0. The load-carrying capacity of C36.H.E60, subjected to an eccentricity of 60 mm, increased by 4.6% while that of C62.H.E60 decreased slightly by 1.4% relative to that of the control. The specimens C36.H.E90 and C62.H.E90 reinforced with grade 600 MPa rebars and subjected to axial loading with an eccentricity of 90 mm experienced peak loads of about 7% higher and 2% lower, respectively, than did the control columns C.36.N.E90 and C62.N.E90. According to Table 4, the specimens C36.H.Ei and C62.H.Ei subjected to infinite eccentricity (under the four-point flexural test) demonstrated an increase of 12.3% and a decrease of 1.1%, respectively, in their maximum load-carrying capacity compared to the corresponding control specimens.

Illustrating the effects of e/h (ratio of load eccentricity level to section width) on load-carrying capacity, Fig. 5 presents percentage enhancements in the load-carrying capacity of specimens reinforced with grade 600 MPa rebars relative to those reinforced with grade 420 MPa rebars. Clearly, load-carrying capacity was not considerably affected by different load eccentricities in specimens made with HSC and reinforced with reduced grade 600 MPa rebars when compared with their counterparts reinforced with NSS rebars. In fact, axial load carrying capacity of HSC columns is dependent on the lateral expansion of columns which is proportional to confinement provision and inversely proportional to unconfined concrete strength [18, 19]. Accordingly, utilizing 600 MPa reinforcing bars was less effective in enhancing the axial load capacity of HSC columns. However, load-carrying capacity increased with increasing load eecentricity to reach 12.3% at infinite eccentricity in specimens made with normal strength concrete (36 MPa) and reinforced with reduced 600 MPa rebars when compared with those containing NSS rebars. Generally speaking, the specimens made with both concrete strengths of 36 and 62 MPa and configured with longitudinal 600 MPa rebar were found comparable with the corresponding reference ones with respect to their load-carrying capacity.

3.3 P–M interaction diagram

Figures 6 and 7 present P–M diagrams for the different categories of specimens subjected to the four

loading eccentricities for comparison of columns reinforced with high-strength rebars and those containing conventional reinforcement in terms of their interactions of axial force and bending moment. Experimental values of maximum axial load and bending moment for all the specimens are reported in Table 4. Moreover, the corresponding theoretical values for the same parameters were calculated using the Whitney equivalent rectangular, force equilibrium equations, and strain compatibility at the column section according to ACI 318-14 [7] guidelines.

Figure 6 presents both the theoretical and experimental P-M interaction diagrams for the specimens reinforced with conventional NSS rebars of Grade 420 MPa and HSS rebars of Grade 600 MPa with two different concrete strengths of 36 MPa and 62 MPa. - Clearly, the calculated values obtained for RC columns subjected to concentric loading underestimated the test results. Smaller differences would have been observed between the computational and the experimental results, if the concrete compressive strength values of the unconfined cylindrical concrete specimens had been replaced in the calculation of loading capacity with those of the "confined" concrete. Although the theoretical estimates above the balanced point in P–M diagrams are more conservative, those below the balanced point are acceptably in agreement with the experimental results, except in the case of C36.N.E60 and C36.N.E90 which recorded experimental load capacities negligibly lower than the estimated values. This confirms the adequacy of the method recommended in ACI-318-14 [7] for the analysis of sections reinforced with high-strength rebars. Obviously, the experimental results in both diagrams in Fig. 6 would converge to those of the theoretical results if load eccentricity increased.

The nondimensional form of the P–M interaction diagram presented in Fig. 7. In this figure maximum axial load and maximum flexural moment were divided by $f'_c A_g$ and $f'_c A_g h$, respectively. Figure 7 indicates that the specimens with concrete strengths of 36 MPa and 62 MPa and reinforced with grade 600 MPa rebars (i.e., groups C36.H and C62.H) have nearly the same axial and moment capacities as those reinforced with 420 MPa steel rebars (groups C36.N and C62.N). However, examination of eccentrically loaded columns in Fig. 7 reveals that specimens reinforced with grade 600 MPa rebars and made with
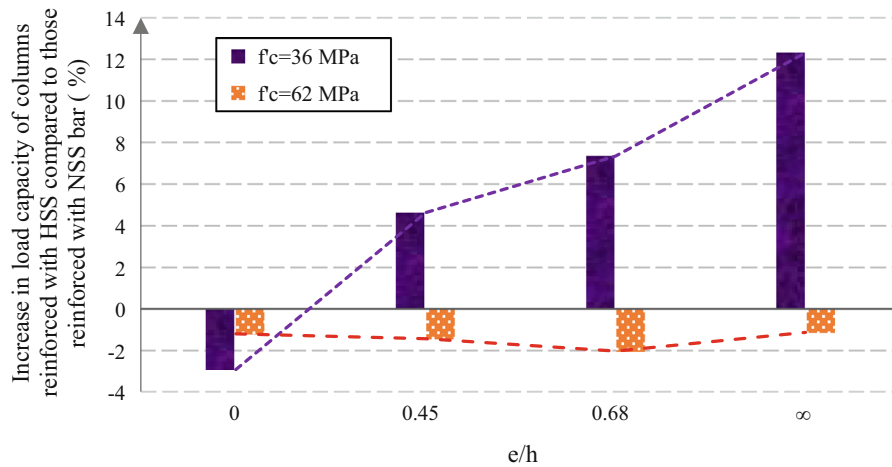
Fig. 5 Increase in load-carrying capacity of column specimens reinforced with HSS bars (600 MPa) in comparison with columns reinforced with NSS rebars at different load eccentricities (e/h)
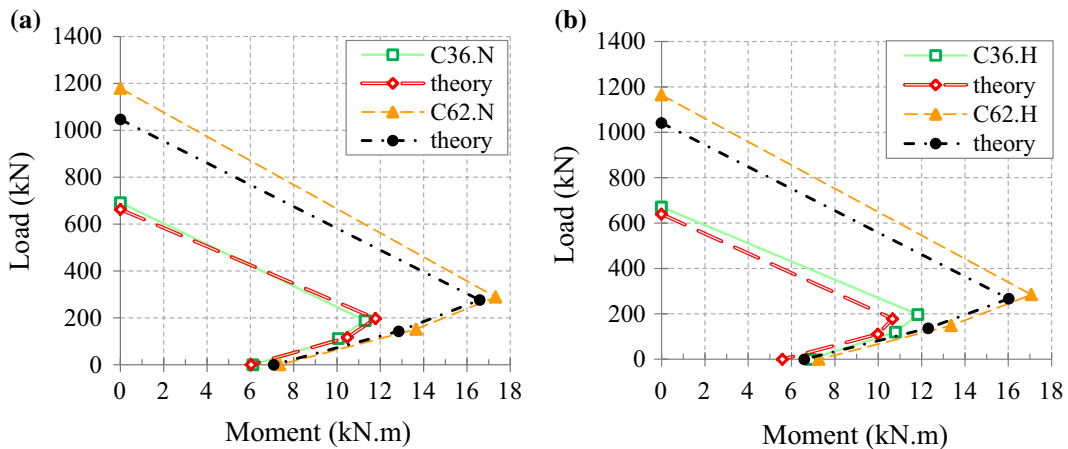

Fig. 6 Theoretical and experimental P–M interaction diagrams for: **a** specimens reinforced with conventional steel rebars (420 MPa); and **b** specimens reinforced with high-strength steel rebars (600 MPa)

normal strength concrete (36 MPa) slightly outperform those containing normal steel strength (420 MPa).

3.4 Ductility

For the purposes of this study, the eccentrically loaded columns reinforced with Grade 420 and 600 MPa rebars were compared using the I_{10} ductility index. Originally due to Foster and Attard [20], the index includes both loading components of axial and flexural forces in ductility measurement of eccentrically loaded columns. In this method, ductility index is defined as the area under the P-ξ curve (Fig. 8)

representing the work accomplished within the column plastic hinge zone by the applied force (P). The parameter ξ denotes the value of "$\varepsilon_{av} + \kappa e$", where ε_{av} is the average value of strains measured on both tension and compression sides of the column, κ is the section curvature, and e is load eccentricity. This may be expressed by Eq. (1) below:

$$I_{10} = \frac{A_2}{A_1} \tag{1}$$

where A_1 and A_2 denote ADE and ABC areas, respectively, in the P–ξ curve (Fig. 8); which are the areas corresponding to the results obtained in the experimental test. As shown in Fig. 8, the procedure
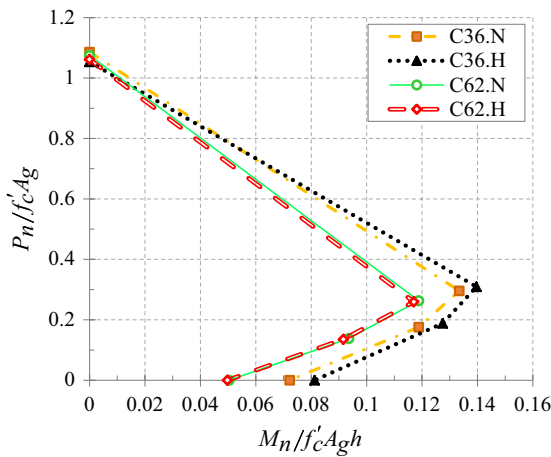
Fig. 7 Comparison of P–M interaction diagrams for the four categories of specimens

adopted herein for the determination of parameter ξ at yield of steel reinforcement, ξ_y, is based on an idealized bilinear force–displacement response with reduced stiffness found at the secant stiffness at either the first yield or at 0.75 of the ultimate load, whichever is less [21]. The values of I_{10} range between 1 and 10, with $I_{10} = 1$ representing an elastic-brittle material and $I_{10} = 10$ indicating a perfectly elasto-plastic one.

The I_{10} ductility values obtained for all the specimens are reported in Table 4. Comparison of the two categories C36.N and C36.H with respect to their ductility index (I_{10}) values revealed that the I_{10} values of the specimens in category C36.H decreased by about 6.4%, 7.7%, and 6.2% when subjected to eccentricities of 0, 90 mm, and infinity, respectively, relative to those for C36.N.E0, C36.N.E90, and
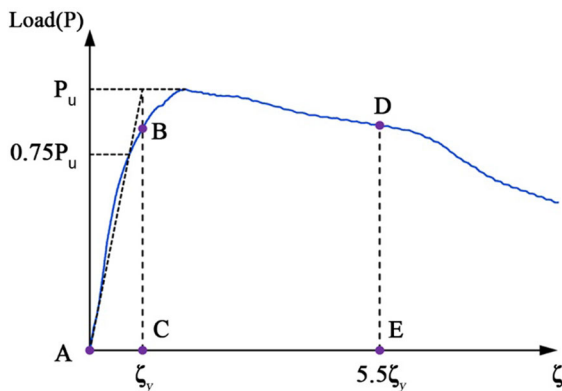

Fig. 8 Energy ductility (I_{10}) measurement

C36.N.Ei. This is while the specimen reinforced with 600 MPa rebars and subjected to a load eccentricity of $e = 60$ mm exhibited a 2.7% increase in its I_{10} value relative to that of the corresponding specimen reinforced with Grade 420 rebars. On the other hand, the simultaneous use of reduced 600 MPa bar and HSC led to ductility indices (I_{10}) higher than that of the control by about 3.5% under the four-point flexural loading test, while the same values reduced in the specimens C62.H.E0, C62.H.E60, and C62.H.E90 by about 7–12% when compared with their corresponding specimens reinforced with Grade 420 MPa rebars. Moreover, the I_{10} values obtained for the specimens reinforced with 600 MPa rebars showed that the use of 62 MPa concrete rather than the 36 MPa one was only effective at higher load eccentricities, i.e., $e = 90$ mm and infinity.

Figure 9 presents the calculated ductility index I_{10} for the four categories of specimens for different e/h (i.e., ratio of load eccentricity to section width). According to this figure, the obtained I_{10} index for all tested columns ranging from 7.2 to 9.1. In the case of concentrically-loaded columns ($e/h = 0$), the value of I_{10} index for C36.H.E0 and C62.H.E0 were 8.5 and 8.4, respectively; which shows 6.4% and 7.7% decrease when compared with their counterparts reinforced with 420 MPa rebars. This indicates that using reduced 600 MPa rebar decreased the ductility (I_{10}) due to a higher likelihood of longitudinal bar buckling.

According to Fig. 9, the value of I_{10} for C36.H.E60 and C62.H.E60 shows 2.8% higher and 12.7% lower value, respectively, when compared with their control specimens. In the case of higher load eccentricity levels, I_{10} values of 7.6, 7.9, 8.1, and 8.5 were calculated for C36.H.E90, C62.H.E90, C36.H.Ei, and C62.H.Ei, respectively.

It may be concluded from the aforementioned description on Fig. 9 that application of 600 MPa rebars has not any negative effect on ductility (i.e., I_{10} index). Moreover, it seems that the 62 MPa high strength concrete was able to slightly affect column behavior under varying load eccentricities; so that better I_{10} values were achieved as e rose above $e/h = 0.45$, while the I_{10} values in specimens containings 600 MPa rebars and 36 MPa concrete decreased slightly compared to the reference ones containing 420 MPa rebars.
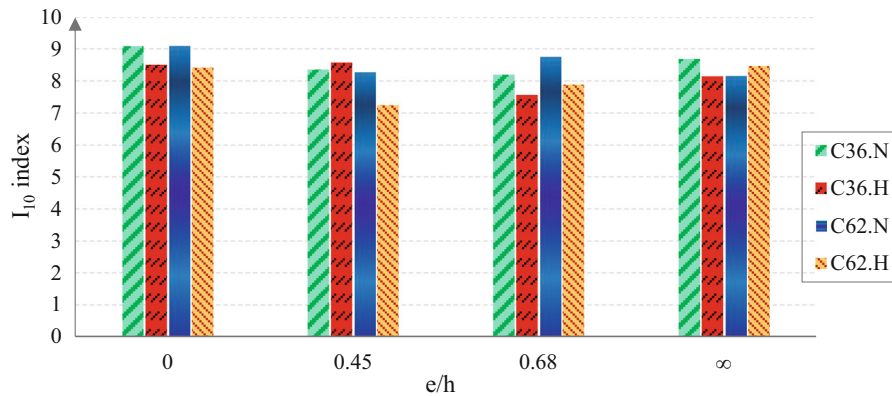
Fig. 9 Effects of load eccentricity (*e/h*) on ductility index (I_{10}) enhancement in comparison with columns reinforced with NSS rebars

It should be noted that the present tests mainly focus on using high strength steel bar in small-sized RC column specimens; however, the size effect might affect the results of actual columns in real structures. In this case, increase in stirrups ratio and yield strength of transverse reinforcement could result in larger triaxial confining pressure which is developed by transverse reinforcement and, consequently, reduces the size effect due to less brittle behavior [22]. On the other hand, mostly eccentrically-loaded columns exhibit weaker size effect than small-eccentrically loaded columns [23].

It is worth mentioning that the presented results demonstrated that using high-strength bars would be applicable in RC columns with normal and high strength concrete, especially if the concrete core is well-confined with transverse reinforcement, and the value of $A_s \cdot f_y$ remains constant; where A_s = area of longitudinal rebars and f_y = yield strength of longitudinal rebars. In the case of NSC specimens, however, utilizing HSS bars in columns designed as tension-controlled section (i.e., where extreme tensile bars yield at ultimate load) would increase the margin of safety regarding axial load capacity.

4 Conclusion

High strength steel (HSS) rebars with a yield strength of 600 MPa were used as longitudinal reinforcement in RC columns to reduce longitudinal bar congestion. For this purpose, 16 experimental RC columns were prepared using two different concrete grades and tested under load eccentricities of 0, 60, 90 mm, and infinity. All the columns with identical grades of concrete strength were designed to have nearly the same flexural capacity and rebar layout. The results of this study are concluded based on the small sizes of the column specimens, and more tests are needed to generalize the results. The following conclusions may be drawn from the results obtained:

1. No considerable difference was observed between the failure mechanisms of the specimens reinforced with 600 MPa rebars and those configured with NSS rebars of grade 420 MPa. Concentrically loaded columns (especially those made of HSC) were failed with sudden concrete cover spalling and crushing followed by longitudinal bar buckling.

2. Using reduced longitudinal 600 MPa rebars effectively led to load carrying capacities and initial stiffness values under varying eccentricities comparable to those obtained for specimens configured with 420 MPa steel rebars. The results acknowledged the idea that the amount of longitudinal reinforcement in a RC column can be reduced by up to 34% if f_y is increased to 600 MPa. In other words, maximum load carrying and initial stiffness are nearly the same if the reduction in column reinforcing bar is proportional to the increase in f_y. Moreover, a good agreement was observed between the experimental and the theoretical values of load-carrying capacity, indicating that column designs based on ACI 318-14 [7] yield reliable results under the maximum loads used in this study.

3. The specimens C36.H.E60 and C62.H.Ei exhibited ductility index (I_{10}) values by 2.7% and 3.5% higher than the corresponding ones reinforced with 420 MPa rebars, repectively, while the use of reduced amounts of longitudinal 600 MPa bar in place of Grade 420 MPa bars led to reductions of 7–12% in ductility index (I_{10}) of other specimens when compared with reference columns. Regarding ductility, the use of high strength concrete coupled with reduced longitudinal 600 MPa rebars was found to be effective only at high load eccentricities (i.e., below the balance point); so that the I_{10} value in C62.H.Ei increased by approximately 4% compared to the corresponding ones configured with Grade 36 MPa concrete strength.

4. Test results showed that increased e/h ratios led to no significant effects on the maximum load carrying of HSC specimens reinforced with 600 MPa rebars in comparison with control columns with 420 MPa rebars; while the load carrying capacity of NSS specimens reinforced with reduced 600 MPa rebars increased up to 12% at $e/h = \infty$ relative to the control specimens reinforced with NSS rebars.

5. Regardless of the longitudinal reinforcement grade employed, the use of high strength concrete with a compression strength of 62 MPa enhanced column yield displacement under low eccentricities (i.e., categories E0 and E60) by approximately 10–28% relative to those made of normal concrete strength (36 MPa). However, the brittle post-peak behavior observed in concentrically loaded columns configured with HSC suggests that concrete cover, different tie configurations, and the ratio of core to section area might play important roles in both yield displacement and post-peak behavior of columns made of high-strength concrete when subjected to concentric loading. Further investigation may be needed to determine their likely roles.

Compliance with ethical standards

Conflict of interest The authors declare that they have no conflict of interest.

References

1. Hognestad E (1961) High strength bars as concrete reinforcement, Part 1—introduction to a series of experimental reports. J PCA Res Develop Lab 3:23–29
2. Richart FE, Brown RL (1934) An investigation of reinforced concrete columns: a report of an investigation. University of Illinois, Engineering Experiment Station, College Station
3. Pfister JF, Mattock AH (1963) High strength bars as concrete reinforcement, part 5—lapped splices in concentrically loaded columns. J PCA Res Develop Lab 5:27–40
4. Todeschini CE, Bianchini AC, Kesler CE (1964) Behavior of concrete columns reinforced with high strength steels. ACI Struct J 61:701–715
5. Nagashima T, Sugano S, Kimura H, Ichikawa A (1992) Monotonic axial compression test on ultra-high-strength concrete tied columns. In: Proceedings of the 10th world conference on earthquake engineering, Madrid, pp 2983–2988
6. ACI Committee 318 (1971) Building code requirements for reinforced concrete, ACI 318-71. American Concrete Institute, Farmington Hills
7. ACI Committee 318 (2014) Building code requirements for structural concrete, ACI 318-14. American Concrete Institute, Farmington Hills
8. ACI Innovation Task Group 6 (2010) Design guide for the use of ASTM A1035/A1035M grade 100 steel bars for structural concrete (ACI ITG-6R-10). American Concrete Institute, Farmington Hills
9. ACI Committee 318 (2008) Building code requirements for reinforced concrete, ACI 318-08. American Concrete Institute, Farmington Hills
10. Shin H-O, Yoon Y-S, Cook WD, Mitchell D (2016) Axial load response of ultra-high-strength concrete columns and high-strength reinforcement. ACI Struct J 113:325
11. Cusson D, Paultre P (1994) High-strength concrete columns confined by rectangular ties. J Struct Eng 120:783–804
12. Pessiki S, Graybeal BA (2000) Axial load tests of concrete compression members with high strength spiral reinforcement. PCI J 45:64–80
13. Martinez S, Nilson AH, Slate FO (1982) Spirally reinforced high strength concrete columns. Cornell University Department of Structural Engineering, Research Report No. 82-10, p 255
14. Nishiyama M, Fukushima I, Watanabe F, Muguruma H (1993) Axial loading tests on high-strength concrete prisms confined by ordinary and high-strength steel. In: Proceedings of the symposium on high strength concrete, Norway, pp 322–329

15. Tamm H (2003) Manual Técnico Thermex-HSE. Hennigsdorf, Hennigsdorfer Stahl Engineering, p 28

16. ACI Committee 211.1 (1991) Proportions for normal, heavyweight, and mass concrete (Reapproved 2009), ACI 211.1-91. American Concrete Institute, Farmington Hills

17. ASTM C39/C39M (2015) Standard test method for compressive strength of cylindrical concrete specimens. ASTM C39/C39M, West Conshohocken

18. Pessiki S, Graybeal B, Mudlock M (2002) Design of high strength spiral reinforcement in concrete compression members. Adv Build Technol 1:431–438

19. Carey SA, Harries KA (2005) Axial behavior and modeling of confined small-, medium-, and large-scale circular sections with carbon fiber-reinforced polymer jackets. ACI Struct J 102:596

20. Foster SJ, Attard MM (1997) Experimental tests on eccentrically loaded high-strength concrete columns. ACI Struct J 94:2295–2303

21. Priestley MJN, Park R (1987) Strength and ductility of concrete bridge columns under seismic loading. ACI Struct J 84:61–76

22. Jin L, Du M, Li D et al (2017) Effects of cross section size and transverse rebar on the behavior of short squared RC columns under axial compression. Eng Struct 142:223–239

23. Xu C, Jin L, Ding Z et al (2016) Size effect tests of high-strength RC columns under eccentric loading. Eng Struct 126:78–91